RSC Advances

PAPER

View Article Online
View Journal | View Issue

Cite this: *RSC Adv.*, 2024, **14**, 7557

Stabilization of the cubic, fast-ion conducting phase of $Li_7La_3Sn_2O_{12}$ garnet by gallium doping†

Hany El-Shinawi, *[ab] Shady M. El-Dafrawy,[a] Mahmoud Tarek,[a] Ahmed F. S. Molouk,[a] Edmund J. Cussen[b] and Serena A. Cussen[b]

All-solid-state batteries present promising high-energy-density alternatives to conventional Li-ion chemistries, and Li-stuffed garnets based on $Li_7La_3Zr_2O_{12}$ (LLZO) remain a forerunner for candidate solid-electrolytes. One route to access fast-ion conduction in LLZO phases is to stabilize the cubic LLZO phase by doping on the Li sites with aliovalent ions such as Al^{3+} or Ga^{3+}. Despite prior attempts, the stabilization of the cubic phase of isostructural $Li_7La_3Sn_2O_{12}$ (LLSO) by doping on the Li sites has up to now not been realised. Here, we report a novel cubic fast-ion conducting $Li_7La_3Sn_2O_{12}$-type phase stabilized by doping Ga^{3+} in place of Li. 0.3 mole of gallium per formula unit of LLSO were needed to fully stabilize the cubic garnet, allowing structural and electrochemical characterizations of the new material. A modified sol–gel synthesis approach is introduced in this study to realise Ga-doping in LLSO, which offers a viable route to preparing new Sn-based candidate solid-electrolytes for all-solid-state battery applications.

Received 31st December 2023
Accepted 27th February 2024

DOI: 10.1039/d3ra08968a

rsc.li/rsc-advances

Introduction

Garnet-type solid-electrolytes possess some of the highest Li-ion conductivities among oxides (up to 1 mS at 25 °C (ref. 1–3)), and the best structural and electrochemical stability among all solid-electrolytes.[4,5] These ceramics are rich in lithium ($Li_{7-x}La_3M_2O_{12}$), with superior ion-transport properties and electrochemical performance linked to compositions based on the parent Li-stuffed garnet $Li_7La_3Zr_2O_{12}$ (LLZO).[6,7] LLZO transforms from a tetragonal phase with poor ion-conducting properties to a cubic phase with fast-ion conducting properties by promoting disorder across the Li sublattice by aliovalent doping at either the Zr and/or the Li sites.[6,7] The cubic modification accommodates a three-dimensional network of open channels for Li^+ transport, typically composed of Li^+ partially-occupied LiO_4 tetrahedra and distorted LiO_6 octahedra sharing faces.[6,7] Doping LLZO at the Zr sites is often associated with a decline in the sinterability and in the overall ionic conductivity, while controlled doping at the Li sites (*e.g.*, with Al and/or Ga) results in phases with improved ionic conductivity and electrochemical performance.[8–10] Al/Ga-doped LLZO has been the subject of extensive studies in the literature,[6,7] which revealed that Al/Ga ions likely occupy the tetrahedral 24d sites in the cubic garnet lattice.[11–14] Isostructural $Li_7La_3Sn_2O_{12}$ (LLSO) exhibits similar structural properties to LLZO,[15] including a tetragonal-to-cubic phase transition upon doping.[16–20] The material, however, is more sensitive to moisture, exhibiting substantial Li^+ exchange with H^+ in ambient air.[21,22] Instability of lithium garnets against humidity is well known and has been widely investigated.[23] Upon storage and/or processing in air at ambient conditions, garnets undergo surface Li^+/H^+ exchange reactions, which result in the formation of resistive Li_2CO_3 surface layers. These layers are often detrimental for the electrochemical performance of lithium garnets in solid-state test cells.[24] H^+-doping in LLZO is also believed to be responsible for the stabilization of the "low-temperature" LLZO phase.[23] In undoped LLSO, Li^+ exchange with H^+ is more significant and results in a spontaneous tetragonal-to-cubic phase transition in ambient air.[21] The cubic "hydrogenated" LLSO phase is, however, poor ion conductor, and cannot be obtained in a suitably dense form. Similar to LLZO, doping at the B-sites (Sn-sites) stabilizes the fast ion-conducting cubic phase of LLSO. Attempts to dope Sn sites with Ta, Nb and Bi have proven successful.[16–20] However, less success has been achieved in doping LLSO at the Li sites[16–19] and a single phase of Al/Ga-doped LLSO is yet to be reported. Al is typically introduced into LLZO at elevated temperatures (>1200 °C).[1] Our previous work has successfully demonstrated that dense Al-doped LLZO phases can be achieved at 1100 °C by sol–gel approaches.[10] Ga-doping in LLZO is also typically achieved at similar temperatures (1100–1200 °C).[9] Unlike LLZO, LLSO is synthesized at relatively low sintering temperatures (~900 °C).[15] Using elevated temperatures to densify the material results in phase destruction and separation of secondary phases such Li_2SnO_3.[15] Hence, the inability to introduce Al^{3+} ions into the

[a]*Department of Chemistry, Faculty of Science, Mansoura University, Mansoura, 35516, Egypt. E-mail: h_elshinawi@mans.edu.eg*

[b]*Department of Materials Science and Engineering, University of Sheffield, Sir Robert Hadfield Building, Sheffield, S1 3JD, UK*

† Electronic supplementary information (ESI) available. See DOI: https://doi.org/10.1039/d3ra08968a

LLSO lattice may be partly related to the insufficient temperature used to synthesize/sinter the material. Similarly, stabilization of cubic LLSO by incorporating Ga^{3+} ions into the garnet lattice has also not been reported. Here, we have employed both solid-state synthesis and a new sol–gel approach to incorporate Ga into LLSO in an attempt to stabilise fast-ion conducting garnet phases based solely on Sn. Garnets based on reducible elements (*e.g.*, Sn, W, Ti, Pr) are currently attracting increasing attention due to their potential applications as interlayers[25,26] or electrode materials[27,28] in all-solid-state batteries. Our results reveal that up to 0.3 mole Ga per LLSO formula unit is required to fully stabilize the cubic phase of LLSO. When a traditional solid-state approach is applied, a Li_2SnO_3 impurity was generally observed. We demonstrate that a single phase of cubic LLSO can be achieved through the use of a modified sol–gel synthesis, enabling structural and electrochemical characterization of this new material.

Experimental section

Synthesis

Solid-state reactions. Lithium carbonate, lanthanum(III) oxide, tin(IV) oxide and gallium(III) oxide were used as the starting materials. Lanthanum oxide was dried at 900 °C for 12 h prior to use. $Li_{7-3x}Ga_xLa_3Sn_2O_{12}$ samples were prepared by mixing stoichiometric amounts of the starting materials (Li : Ga : La : Sn molar ratios of $7-3x : x : 3 : 2$), where $x = 0.1$, 0.2, 0.3, 0.4, 0.5 and 0.6, and using 10 mol% excess of Li in each case. The materials were intimately ground for 30 min using a pestle and mortar, followed by pre-calcination at 700 °C for 12 h. The produced powders were pressed into pellets (at ~250 MPa), and finally calcined at 900 °C for 12 h.

Modified sol–gel synthesis. Lithium acetate, lanthanum(III) oxide, tin(IV) *tert*-butoxide and gallium(III) acetylacetonate were used as the starting materials (Li : Ga : La : Sn molar ratios of $7-3x : x : 3 : 2$, where $x = 0.2$ and 0.3). Lithium, lanthanum and gallium compounds were dissolved in dilute nitric acid (2 wt%) at ~80 °C. An equivalent amount of citric acid (total metal ions to citric acid molar ratio of 1 : 2) was added to the metal ion solution (solution A). A stoichiometric amount of tin(IV) *tert*-butoxide was weighed out in a beaker in an argon-filled glovebox, then transferred to a fumehood, where it was dissolved in an NH_3/H_2O_2 (1 : 1, vol/vol) solution at ~80 °C (solution B). Solutions A and B were carefully mixed resulting in a clear solution of pH ~7. This solution was then slowly evaporated at 80 °C. The produced gel was auto-combusted when the temperature was increased to 200 °C. The obtained ash was heated at 550 °C overnight to remove organics, then the produced white powder was finally calcined at 900 °C for 6 h. To prepare pellets for the impedance measurements, the powder calcined at 550 °C was uniaxially pressed into pellets before calcination at 900 °C for 6 h. To prepare more dense pellets, the powders calcined at 900 °C were hot-pressed into 13 mm diameter cylindrical ingots for 10 min at 950 °C and ~50 MPa. The density of the sintered pellets was calculated using the mass and the geometry of the bulk material, and compared to the theoretical density deduced from Rietveld refinement of the diffraction data.

Characterization

X-ray diffraction (XRD) studies were performed using a Rigaku Miniflex diffractometer with a Cu Kα X-ray source. Rietveld fits to XRD data were done using the GSAS and EXPGUI suite of programmes. ICP-MS analysis was performed using a Thermo Scientific iCAP RQplus ICP-MS instrument. SEM/EDX studies were conducted using an FEI Inspect F50 high resolution electron microscope. AC impedance and DC polarization measurements were conducted in Swagelok cells assembled under argon atmosphere, and the data were recorded using Biologic VMP-300 potentiostat. AC impedance data were recorded in the frequency range of 1 MHz to 1 Hz (an electrical perturbation of 50 mV) using gold or lithium electrodes. Prior to each impedance measurement, the samples were equilibrated for 1 h at constant temperature. DC polarization measurements were performed on samples with gold electrodes by applying voltages in the range of 0.7–1.9 V (8 hours each) and recording the corresponding DC current. Gold electrodes were gas-phase deposited on the circular sides of the pellets by thermal evaporation. To prepare lithium symmetric cells, pellets were sandwiched between two Li foils, pressed at ~12.5 MPa, and assembled within a Swagelok cell in an argon-filled glovebox. Lithium foil was scraped using a stainless-steel blade before use to ensure a clean surface.

Results and discussion

Conventional solid-state reactions were first employed to synthesize Ga-doped LLSO materials with Ga/LLSO molar ratios of 0.1, 0.2, 0.3, 0.4, 0.5 and 0.6. The XRD patterns collected from these materials are represented in Fig. 1a. A smooth transformation from tetragonal to cubic symmetry was initially observed upon increasing the ratio of the Ga dopant. 0.3 mole of Ga per formula unit of LLSO is found to be sufficient to fully stabilize the cubic garnet phase, as indicated from the absence of peak broadening/splitting. A further increase of the molar ratio of the Ga dopant (>0.4) resulted in a destruction of the cubic phase and the appearance of a $LiGaO_2$ impurity, indicating an excess of Ga. For all samples prepared *via* the traditional solid-state route, traces of a second phase of Li_2SnO_3 were apparent regardless of the molar ratio employed. Attempts to reduce or remove this phase by applying different sintering temperatures (950–1050 °C), sintering times, and/or quenching procedures, were unsuccessful. Nevertheless, the results suggest that the minimum amount of Ga dopant required to stabilize the cubic modification of the LLSO garnet, and is therefore likely introduced into the garnet lattice, is ~0.3 mole. This is in a good agreement with our studies on the isostructural LLZO phase, which showed a very similar tetragonal-to-cubic transition upon increasing the amount of the Ga dopant.[9] However, it is worth noting that in the case of LLZO, the excess gallium (>0.4 mole per formula unit of LLZO) appeared as a $LiGaO_2$ impurity and no phase destruction was

observed.[9] The $LiGaO_2$ acted as a sintering aid and helped to stabilize cubic LLZO, which is not observed here for LLSO.

Rietveld refinement of powder XRD data of 0.3Ga-doped LLSO, employing a standard cubic garnet structure model with Ga^{3+} occupying the tetrahedral 24d crystal sites,[13,14] indicates the presence of 3.0(1) wt% of Li_2SnO_3 impurity. Fig. 1b shows the fitted XRD pattern of the 0.3Ga-doped LLSO sample synthesized *via* the solid-state route. The structural parameters used in the refinement are summarized in Table S1.† To improve the purity of this phase, a new sol–gel synthetic procedure was introduced. In sol–gel synthesis, the reacting species are mixed on the atomic scale which helps to achieve complete solid-state reactions at lower sintering temperatures. This is favoured for LLSO, as a sintering temperature as low as

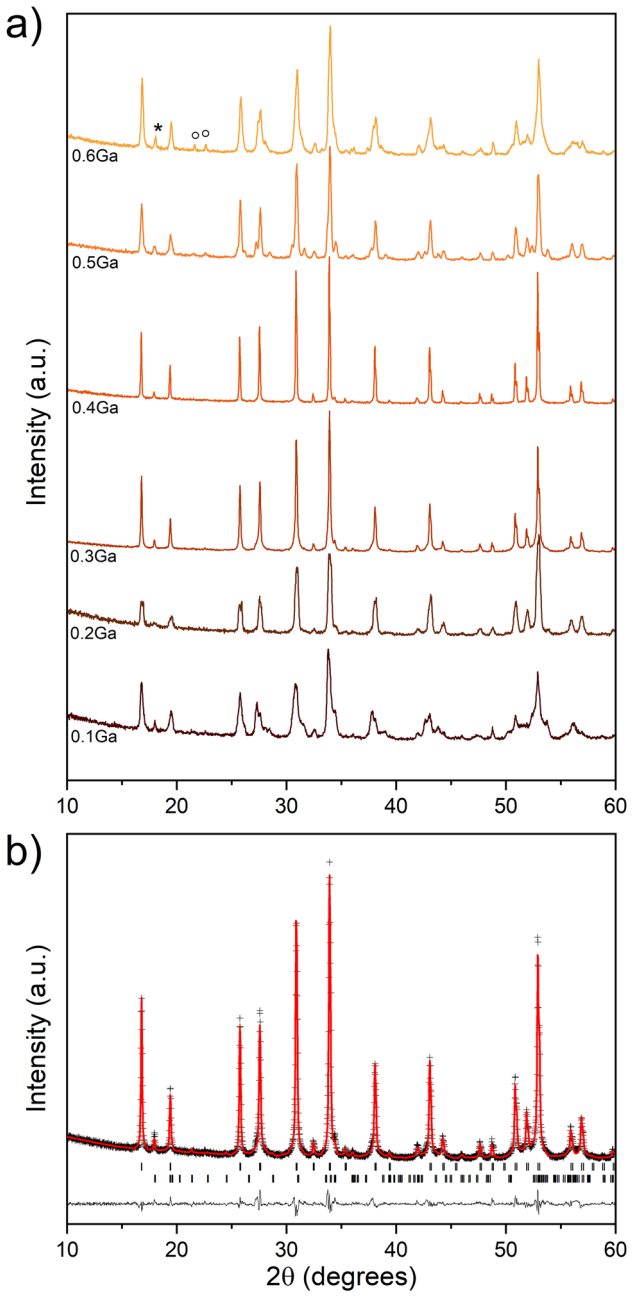

Fig. 1 XRD data of Ga-doped LLSO synthesized by solid-state reactions. (a) XRD patterns of samples with Ga/LLSO molar ratios of 0.1, 0.2, 0.3, 0.4, 0.5 and 0.6. * and ° denote traces of Li_2SnO_3 and $LiGaO_2$ impurities, respectively. (b) Rietveld refinement of the XRD data of 0.3Ga-doped LLSO, indicating the main garnet phase and traces of Li_2SnO_3 as a secondary phase.

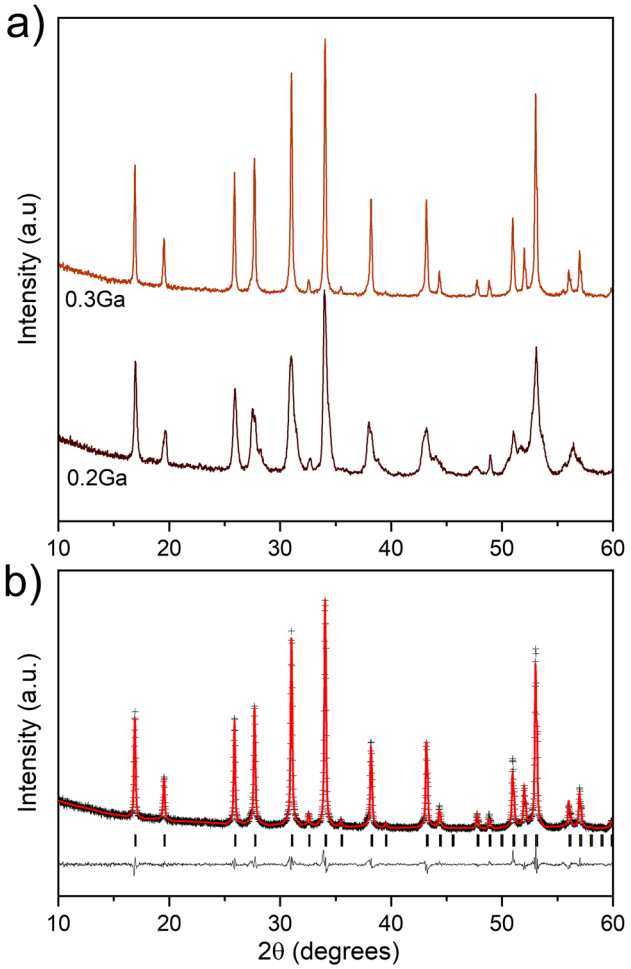

Fig. 2 XRD data of Ga-doped LLSO synthesized by sol–gel technique. (a) XRD patterns of samples with Ga/LLSO molar ratios of 0.2 and 0.3. (b) Rietveld refinement of the XRD data of 0.3Ga-doped LLSO.

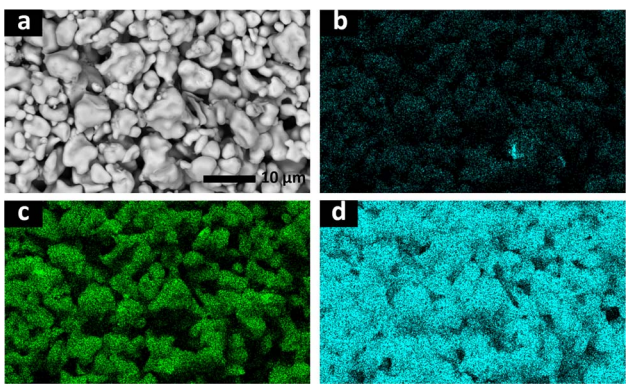

Fig. 3 SEM image (a) and EDX elemental maps collected from the surface of a pellet of 0.3Ga-doped LLSO, showing the distribution of gallium (b), tin (c) and lanthanum (d).

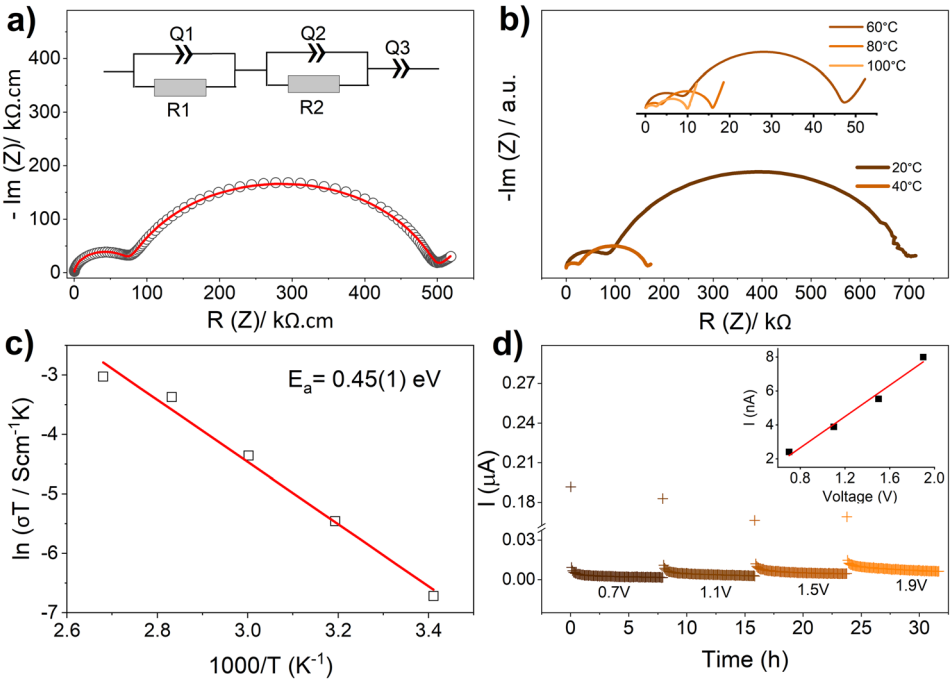

Fig. 4 (a) The impedance plot of 0.3Ga-doped LLSO at 40 °C, fitted using the [R1Q1][R2Q2][Q3] equivalent circuit (the inset). (b) Typical impedance plots of 0.3Ga-doped LLSO at different temperatures. (c) The Arrhenius plot for the bulk conductivity of 0.3Ga-doped LLSO in the temperature range 20–100 °C. (d) DC polarization curves (at 40 °C) of 0.3Ga-doped LLSO at different voltages (0.7–1.9 V) and the corresponding I/V plot (the inset).

900 °C is crucial. Fig. 2a shows the XRD patterns of sol–gel-synthesized 0.2Ga-doped and 0.3Ga-doped LLSO, indicating the disappearance of the Li_2SnO_3 impurity and the formation of a single phase of the cubic garnet in the case of 0.3Ga-doped LLSO. ICP-MS analysis of 0.3Ga-doped LLSO indicated that the La : Ga molar ratio is 3 : 0.286(6), which is in good agreement with the reaction stoichiometry (3 : 0.3). SEM images showed smaller particle sizes than those observed in the sample synthesized by solid-state reactions (Fig. S1†). EDX elemental maps revealed a homogeneous distribution of Ga across the material (Fig. 3), which suggests that Ga is incorporated in the garnet lattice with no significant secondary-phase formation. Rietveld refinement of the XRD data of 0.3Ga-doped LLSO was employed using a standard cubic garnet structure with Li^+ distributed between tetrahedral 24d and distorted octahedral 96 h sites, and Ga^{3+} partially occupying the 24d sites.[13,14] The Ga-content was fixed at 0.285 mole per unit formula of LLSO, as determined from ICP-MS. The refinement (Fig. 2b) revealed a unit cell parameter ***a*** of 12.9522(4) Å. The structural parameters used in the refinement are summarized in Table S2.† The material showed no evidence of significant phase modifications after storage in air (Fig. S2†).

Ga-doping has therefore been achieved in LLSO yielding a cubic garnet-type phase. It is worth mentioning that stabilising the cubic LLSO phase without doping on the B-sites (Sn site) has not previously been reported. The electrochemical properties of this new material were studied by impedance spectroscopy and DC polarization tests. Pellets obtained directly from the synthesis step (*i.e.*, sintered at 900 °C) and employing sputter-coated gold electrodes, were used in these studies. The impedance plot collected from 0.3Ga-doped LLSO at 40 °C is presented in Fig. 4a. The impedance consisted of two semicircles at high and intermediate frequencies followed by an incomplete spike at low frequencies. The appearance of a low-frequency spike, which appears more pronounced at higher temperatures, on using blocking gold electrodes suggests that the charge transfer in the material is mainly ionic. The impedance data were well described by an equivalent circuit that employs a constant phase element (Q) in parallel to a resistance element (R) to represent a semicircle ([RQ]), and a constant phase element to represent the low frequency spike ([Q]). The capacitances (C) calculated from the fit parameter Q of the high-frequency and intermediate-frequency semicircles are 7.5×10^{-12} and 6.7×10^{-9} F, respectively. These values are in excellent agreement with the capacitances expected from bulk and grain-boundary effects, respectively.[29,30] The high frequency semicircle was therefore associated to the bulk resistance of the material and the intermediate-frequency semicircle was associated to the grain boundary resistance of the material. The fitted data suggest that the bulk and total conductivities of the material are 1.4×10^{-5} and 2.0×10^{-6} S cm^{-1}, respectively. Hence, the total conductivity is almost one order of magnitude lower than the bulk conductivity, indicating a significant contribution from the grain-boundary resistance to the total resistance of the material. This is consistent with insufficient sintering of the material achieved at sintering temperatures as low as 900 °C. Interestingly, the bulk conductivity of the material is increased to $\sim 1 \times 10^{-4}$ S cm^{-1} (*i.e.*, fast-ion conducting

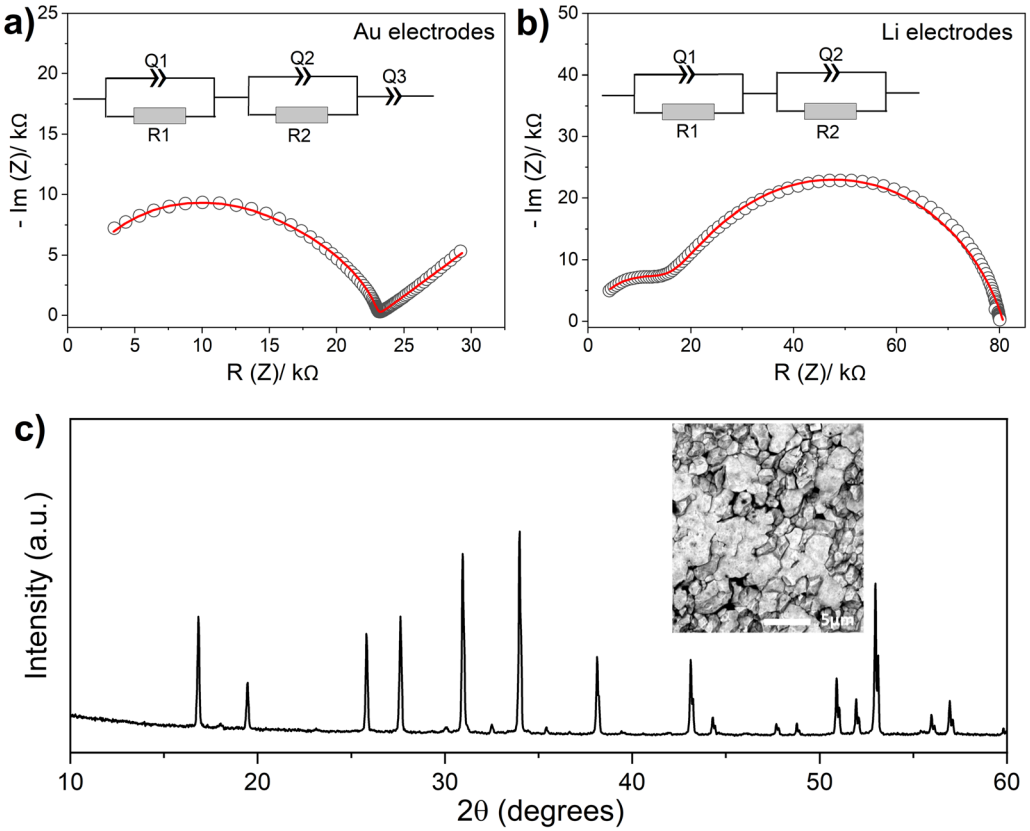

Fig. 5 (a) The impedance plot of hot-pressed 0.3Ga-doped LLSO collected at 40 °C using gold electrodes, and fitted using the [*R*1*Q*1][*R*2*Q*2][*Q*3] equivalent circuit (the inset). (b) The impedance plot of hot-pressed 0.3Ga-doped LLSO collected at 40 °C using lithium electrodes, and fitted using the [*R*1*Q*1][*R*2*Q*2] equivalent circuit (the inset). (c) XRD pattern and SEM image (the inset) of hot-pressed 0.3Ga-doped LLSO.

properties) when the impedance measurement temperature is increased to 80 °C. The bulk conductivity is hence approximately two orders of magnitude higher than that of undoped LLSO (~2.8×10^{-7} S cm^{-1} at room temperature[19]) and comparable to the bulk conductivities observed for Ta-doped LLSO (~1–50 $\times 10^{-6}$ S cm^{-1} (ref. 19)). The impedance spectra of undoped LLSO and 0.3Ga-doped LLSO samples are compared in Fig. S3.† Impedance data collected at different temperatures in the range 20–100 °C (Fig. 4b) are used to estimate the activation energy (E_a) of ion transport in 0.3Ga-doped LLSO using the Arrhenius plot (Fig. 4c) of $\sigma = \sigma_0 \exp(-E_a/kT)$, where σ_0 is the pre-exponential factor, k is the Boltzmann constant, T is the absolute temperature. An activation energy for the bulk ion conductivity of 0.45(1) eV was obtained. This value is consistent with the values reported for cubic LLSO-type phases stabilized by doping with Ta at Sn-sites (~0.4–0.5 eV (ref. 17–19)). DC polarization tests were employed to evaluate any significant contribution of the electronic conductivity to the measured conductivity, by applying voltages in the range of 0.7–1.9 V for up to 32 h (Fig. 4d). These tests revealed an electronic conductivity of 4.6×10^{-9} S cm^{-1} at 40 °C, which clearly suggests that the observed conductivity of the new material (2.0×10^{-6} S cm^{-1} at the same temperature) is mainly ionic.

Attempts to densify Ga-doped LLSO samples through sintering at temperatures greater than 1000 °C resulted in significant phase decomposition (Fig. S4†). To prepare more dense material, a sample of phase-pure 0.3Ga-doped LLSO was hot-pressed at 950 °C. Higher densification temperatures were avoided to alleviate any significant phase decompositions. The hot-pressed sample revealed a relative density of 88% compared with 69% for the cold-pressed sample, indicating a significant improvement of the sinterability of the material by hot pressing. Fig. 5c shows the XRD pattern and SEM image collected from the densified material, confirming the material retains the cubic garnet structure and clearly shows better sinterability compared with the cold-pressed sample (Fig. 3a). Fig. 5c shows the emergence of small impurities of La_2O_3 and Li_2SnO_3 as a result of the heating process. These impurities, however, are present in negligible amounts that apparently will not affect the subsequent impedance analyses. Fig. 5a shows the impedance plot collected from the hot-pressed sample at 40 °C. The plot is formed of one distorted semicircle and a low frequency spike. The presence of the low frequency spike again accounts for an ionic-type conduction. The distorted semicircle clearly accounts for the total resistance of the material, and the plot could be fitted using the same equivalent circuit used for the impedance data of the cold-pressed sample ([*R*1*Q*1][*R*2*Q*2][*Q*3]). The obtained refined parameters are R1 = 14.2 kΩ ($C1 = 5.7 \times 10^{-11}$ F) and $R2$ = 8.8 kΩ ($C2 = 6.3 \times 10^{-9}$ F). The grain-boundary resistance ($R2$) is clearly minimized compared to the bulk

resistance ($R1$) due to improved sinterability of the material. The total conductivity of 0.3Ga LLSO at 40 °C has therefore improved to 1.1×10^{-5} S cm^{-1} upon densifying the material.

Obtaining a dense material of 0.3Ga-doped LLSO by hot-pressing allowed for the testing of a symmetric cell of the material using Li electrodes (Li/0.3Ga-LLSO/Li). Li electrodes were successfully attached to the garnet pellet surfaces by applying a small uniaxial pressure (~0.1 ton) at room temperature. The impedance collected from the symmetric cell at 40 °C is shown in Fig. 5b and consists of two semicircles. The absence of a low frequency spike is consistent with the use of non-blocking Li electrodes and with the observation that the transport properties are mainly ionic. The resistance measured from the first (high-frequency) semicircle agrees well with the total resistance of the pellet as determined using gold electrodes. Hence, the second semicircles accounts for the charge transfer at the Li/garnet interface.[9,10] The impedance plot is successfully fitted using the equivalent circuit [$R1Q1$][$R2Q2$], with a capacitance of 1.8×10^{-8} F associated to the second (low-frequency) semicircle. The latter value is characteristic of an electrode effect[29,30] and further confirms that the low frequency semicircle is associated with the interfacial resistance at the Li/garnet interface. This interfacial resistance is highly dependent on how well the Li metal and garnet are in contact, as well as the stability of the garnet surface against lithium. The large interfacial resistance observed in Fig. 5b (~50 kΩ cm^2) suggests that the Li/LLSO interface is highly resistive under our experimental conditions. The interfacial resistance, however, was not increasing with time, which indicates a stable interface. Moreover, a noticeable reduction of the size of the low frequency semicircle was observed after 12 hours (Fig. S5†), which possibly indicates the formation of a lithiated LLSO interphase that allows Li ion transport. Similar effects have been observed in W-doped LLZO due to reduction of W^{6+} ions.[31] A symmetric Li/0.3Ga-LLSO/Li cell could be cycled at relatively low current density (200 μA cm^{-2}), showing a stable cycle performance (Fig. S6†), however, a less stable performance followed by short-circuiting were observed at higher current densities (*e.g.*, 400 μA cm^{-2}). Further studies are required to characterize the Li/Ga-LLSO interface.

Conclusions

The cubic, fast-ion conducting modification of $Li_7La_3Sn_2O_{12}$ is successfully stabilized by doping the material with gallium. This is the first cubic $Li_7La_3Sn_2O_{12}$-type phase which could be stabilized with no doping at the B-sites (Sn sites). 0.3 mole Ga per formula unit of $Li_7La_3Sn_2O_{12}$ is found to be sufficient to stabilize the cubic garnet phase. A novel sol–gel synthetic approach was employed to obtain the material as a single phase. Based on XRD data analysis, a lattice parameter ***a*** of 12.9522(4) Å is observed for the 0.3Ga-doped sample, where Ga was successfully accommodated at the Li (24d) sites. The charge transport in the material is mainly ionic with no significant contribution from electronic conductivity, as indicated from the DC polarization measurements. The material shows bulk ion conductivities of 1.4×10^{-5} S cm^{-1} and 0.9×10^{-4} S cm^{-1} at 40 and 80 °C, respectively. An activation energy for the bulk conductivity of 0.45(1) eV was observed in the temperature range 20–100 °C. The new material is successfully densified by hot-pressing, with no significant effect on the phase purity, showing a total conductivity of 1.1×10^{-5} S cm^{-1} at 40 °C. The interface between Li and Ga-LLSO is resistive but the resistance does not grow with time, indicating a stable Li/Ga-LLSO interface.

Conflicts of interest

There are no conflicts of interest to declare.

Acknowledgements

This work was supported by the ICSF Faraday Challenge project SOLBAT, UK [grant FIRG007], and the Academy of Scientific Research and Technology, Egypt [grant RESPECT-10025].

References

1 R. Murugan, V. Thangadurai and W. Weppner, Fast lithium ion conduction in garnet-type Li7La3Zr2O12, *Angew. Chem., Int. Ed.*, 2007, **46**, 7778–7781.
2 Y. Li, J. T. Han, C. A. Wang, H. Xie and J. B. Goodenough, Optimizing Li+ conductivity in a garnet framework, *J. Mater. Chem.*, 2012, **22**, 15357–15361.
3 D. Rettenwander, G. Redhammer, F. Preishuber-Pflügl, L. Cheng, L. Miara, R. Wagner, A. Welzl, E. Suard, M. M. Doeff, M. Wilkening, J. Fleig and G. Amthauer, Structural and Electrochemical Consequences of Al and Ga Cosubstitution in Li7La3Zr2O12 Solid Electrolytes, *Chem. Mater.*, 2016, **28**, 2384–2392, DOI: 10.1021/acs.chemmater.6b00579.
4 V. Thangadurai, D. Pinzaru, S. Narayanan and A. K. Baral, Fast solid-state Li ion conducting garnet-type structure metal oxides for energy storage, *J. Phys. Chem. Lett.*, 2015, **6**, 292–299.
5 T. Thompson, S. Yu, L. Williams, R. D. Schmidt, R. Garcia-Mendez, J. Wolfenstine, J. L. Allen, E. Kioupakis, D. J. Siegel and J. Sakamoto, Electrochemical Window of the Li-Ion Solid Electrolyte Li7La3Zr2O12, *ACS Energy Lett.*, 2017, **2**, 462–468, DOI: 10.1021/acsenergylett.6b00593.
6 C. Wang, K. Fu, S. P. Kammampata, D. W. McOwen, A. J. Samson, L. Zhang, G. T. Hitz, A. M. Nolan, E. D. Wachsman, Y. Mo, V. Thangadurai and L. Hu, Garnet-Type Solid-State Electrolytes: Materials, Interfaces, and Batteries, *Chem. Rev.*, 2020, **120**(10), 4257–4300, DOI: 10.1021/acs.chemrev.9b00427.
7 A. J. Samson, K. Hofstetter, S. Bag and V. Thangadurai, A bird's-eye view of Li-stuffed garnet-type Li7La3Zr2O12 ceramic electrolytes for advanced all-solid-state Li batteries, *Energy Environ. Sci.*, 2019, **12**(10), 2957–2975.
8 S. Qin, X. Zhu, Y. Jiang, M. E. Ling, Z. Hu and J. Zhu, Growth of self-textured Ga3+-substituted Li7La3Zr2O12 ceramics by solid state reaction and their significant enhancement in ionic conductivity, *Appl. Phys. Lett.*, 2018, **112**, 113901.

9 H. El-Shinawi and J. Janek, Stabilization of cubic lithium-stuffed garnets of the type "Li7La3Zr2O12" by addition of gallium, *J. Power Sources*, 2013, **225**, 13.
10 H. El-Shinawi, G. W. Paterson, D. MacLaren, E. J. Cussen and S. A. Corr, Low-temperature densification of Al-doped Li7La3Zr2O12: a reliable and controllable synthesis of fast-ion conducting garnets, *J. Mater. Chem. A*, 2017, **5**, 319.
11 H. Buschmann, J. Dölle, S. Berendts, A. Kuhn, P. Bottke, M. Wilkening, P. Heitjans, A. Senyshyn, H. Ehrenberg, A. Lotnyk, V. Duppel, L. Kienle and J. Janek, Structure and dynamics of the fast lithium ion conductor "Li7La3Zr2O12", *Phys. Chem. Chem. Phys.*, 2011, **13**, 19378–19392.
12 D. Wang, G. Zhong, O. Dolotko, Y. Li, M. J. McDonald, J. Mi, R. Fu and Y. Yang, The synergistic effects of Al and Te on the structure and Li+-mobility of garnet-type solid electrolytes, *J. Mater. Chem. A*, 2014, **2**, 20271–20279.
13 M. A. Howard, O. Clemens, E. Kendrick, K. S. Knight, D. C. Apperly, P. A. Anderson and P. R. Slater, Effect of Ga incorporation on the structure and Li ion conductivity of La3Zr2Li7O12, *Dalton Trans.*, 2012, **41**, 12048–12053.
14 C. Bernuy-Lopez, W. J. Manalastas, J. M. L. Del Amo, A. Aguadero, F. Aguesse and J. A. Kilner, Atmosphere Controlled Processing of Ga-Substituted Garnets for High Li-Ion Conductivity Ceramics, *Chem. Mater.*, 2014, **26**, 3610–3617.
15 J. Percival, E. Kendrick, R. I. Smith and P. R. Slater, Cation ordering in Li containing garnets: synthesis and structural characterisation of the tetragonal system, Li7La3Sn2O12, *Dalton Trans.*, 2009, 5177–5181.
16 K. Saranya, C. Deviannapoorani, L. Dhivya, S. Ramakumar, N. Janani and R. Murugan, Li7-xLa3Sn2-xNbxO12 (x = 0.25–1) cubic lithium garnet, *Mater. Lett.*, 2012, **77**, 57–59, DOI: **10.1016/j.matlet.2012.03.002**.
17 C. Deviannapoorani, S. Ramakumar and R. Murugan, Phase transition, lithium ion conductivity and structural stability of tin substituted lithium garnets, *RSC Adv.*, 2016, **6**, 94706.
18 N. Hamao, K. Kataoka and J. Akimoto, Li-ion conductivity and crystal structure of garnet-type Li6.5La3M1.5Ta0.5O12 (M = Hf, Sn) oxides, *J. Ceram. Soc. Jpn.*, 2017, **125**, 272–275, DOI: **10.2109/jcersj2.16273**.
19 L. Ladenstein, S. Simic, G. Kothleitner, D. Rettenwander and H. M. R. Wilkening, Anomalies in Bulk Ion Transport in the Solid Solutions of Li7La3M2O12 (M = Hf, Sn) and Li5La3Ta2O12, *J. Phys. Chem. C*, 2020, **124**(31), 16796–16805, DOI: **10.1021/acs.jpcc.0c03558**.
20 R. J. Pei, Y. F. Li, T. Song, N. Chen and R. Yang, A solid composite electrolyte of 3D framework Li6.25La3Sn1.25Bi0.75O12 for rechargeable solid-state batteries, *J. Alloys Compd.*, 2023, **933**, 167639, DOI: **10.1016/j.jallcom.2022.167639**.
21 C. Galven, J.-L. Fourquet, M.-P. Crosnier-Lopez and F. L. Berre, Instability of the Lithium Garnet Li7La3Sn2O12: Li+/H+ Exchange and Structural Study, *Chem. Mater.*, 2011, **23**(7), 1892–1900, DOI: **10.1021/cm103595x**.
22 C. Galven, J. Dittmer, E. Suard, F. L. Berre and M. P. Crosnier-Lopez, Instability of Lithium Garnets against Moisture. Structural Characterization and Dynamics of Li7-xHxLa3Sn2O12 and Li5-xHxLa3Nb2O12, *Chem. Mater.*, 2012, **24**(17), 3335–3345, DOI: **10.1021/cm300964k**.
23 R. Ye, M. Ihrig, N. Imanishi, M. Finsterbusch and E. Figgemeier, A Review on Li+/H+ Exchange in Garnet Solid Electrolytes: From Instability against Humidity to Sustainable Processing in Water, *ChemSusChem*, 2021, **14**, 4397–4407.
24 A. Sharafi, E. Kazyak, A. L. Davis, S. Yu, T. Thompson, D. J. Siegel, N. P. Dasgupta and J. Sakamoto, Surface Chemistry Mechanism of Ultra-Low Interfacial Resistance in the Solid-State Electrolyte Li7La3Zr2O12, *Chem. Mater.*, 2017, **29**, 7961–7968.
25 G. V. Alexander, C. Shi, J. O'Neill and E. D. Wachsman, Extreme lithium-metal cycling enabled by a mixed ion- and electron-conducting garnet three-dimensional architecture, *Nat. Mater.*, 2023, **22**, 1136, DOI: **10.1038/s41563-023-01627-9**.
26 J. Gao, J. Zhu, X. Li, J. Li, X. Guo, H. Li and W. Zhou, Rational Design of Mixed Electronic-Ionic Conducting Ti-Doping Li7La3Zr2O12 for Lithium Dendrites Suppression, *Adv. Funct. Mater.*, 2020, **31**, 2001918, DOI: **10.1002/adfm.202001918**.
27 R. Satish, V. Aravindan, W. C. Ling, J. B. Goodenough and S. Madhavi, Carbon-Coated Li3Nd3W2O12: A High Power and Low-Voltage Insertion Anode with Exceptional Cycleability for Li-Ion Batteries, *Adv. Energy Mater.*, 2014, **4**, 1301715, DOI: **10.1002/aenm.201301715**.
28 H. Xie, K.-S. Park, J. Song and J. B. Goodenough, Reversible lithium insertion in the garnet framework of Li3Nd3W2O12, *Electrochem. Commun.*, 2012, **19**, 135, DOI: **10.1016/j.elecom.2012.03.014**.
29 J. T. S. Irvine, D. C. Sinclair and A. R. West, Electroceramics Characterization by Impedance Spectroscopy, *Adv. Mater.*, 1990, **2**, 132.
30 W. B. Reid and A. R. West, Atmospheric attack on lithium silicate glass, *Solid State Ionics*, 1988, **28–30**, 681–686.
31 I. McClelland, H. El-Shinawi, S. Booth, A. Regoutz, J. Clough, S. Altus, E. J. Cussen, P. Baker and S. A. Cussen, The Role of the Reducible Dopant in Solid Electrolyte–Lithium Metal Interfaces, *Chem. Mater.*, 2022, **34**, 5054.